

The dependence of galaxy group star formation rates and metallicities on large scale environment.

Jillian M. Scudder^{1*}, Sara L. Ellison¹, J. Trevor Mendel¹

¹ *Department of Physics and Astronomy, University of Victoria, Victoria, British Columbia, V8P 1A1, Canada.*

31 October 2018

ABSTRACT

We construct a sample of 75,863 star forming galaxies with robust metallicity and star formation rate measurements from the Sloan Digital Sky Survey Data Release 7 (SDSS DR7), from which we select a clean sample of compact group (CG) galaxies. The CGs are defined to be close configurations of at least 4 galaxies that are otherwise apparently isolated. Our selection results in a sample of 112 spectroscopically identified compact group galaxies, which can be further divided into groups that are either embedded within a larger structure, such as a cluster or large group, or truly isolated systems. The compact groups then serve as a probe into the influence of large scale environment on a galaxy’s evolution, while keeping the local density fixed at high values. We find that the star formation rates (SFRs) of star forming galaxies in compact groups are significantly different between isolated and embedded systems. Galaxies in isolated systems show significantly enhanced SFR, relative to a control sample matched in mass and redshift, a trend not seen in the embedded systems. Galaxies in isolated systems exhibit a median SFR enhancement at fixed stellar mass of $+0.07 \pm 0.03$ dex. These dependences on large scale environment are small in magnitude relative to the apparent influence of local scale effects found in previous studies, but the significance of the difference in SFRs between our two samples constrains the effect of large scale environment to be non-zero. We find no significant change in the gas-phase interstellar metallicity for either the isolated or embedded compact group sample relative to their controls. However, simulated samples that include artificial offsets indicate that we are only sensitive to metallicity changes of $\log O/H > 0.13$ dex (at 99% confidence), which is considerably larger than the typical metallicity differences seen in previous environmental studies.

Key words: galaxies: interactions, galaxies: groups: general, galaxies: evolution, galaxies: abundances

1 INTRODUCTION

The evolution of a galaxy is fundamentally shaped by its environment. Qualitative evidence of the influence of environment has been known since the 1930s (e.g., Hubble & Humason 1931); the large surveys now available have added their statistical weight to its influence, allowing a quantification of environmental changes. Nearly every observable quantity of a galaxy has been shown to vary with environment, including star formation rates (SFRs), morphologies, colours, active galactic nucleus (AGN) fractions, and mean stellar mass (e.g., Dressler 1980; Balogh et al. 2004; Kauffmann et al. 2004; Croton et al. 2005; Baldry et al. 2006; Park et al. 2007). The primary mechanisms that can operate in denser environments are strangulation, harassment, and ram-pressure stripping (e.g., Gunn & Gott 1972; Larson et al. 1980; Moore et al. 1996). However, disentangling which of these might be a fundamental

variable and which are corollary effects is a non-trivial task (e.g., Whitmore & Gilmore 1991; Blanton et al. 2005; Blanton & Berlind 2007; Skibba et al. 2009). Moreover, relatively simple processes such as individual galaxy–galaxy interactions become complicated by the influence of a local, high density environment. For example, at low densities, close galaxy pairs show enhanced SFRs (Lambas et al. 2003; Alonso et al. 2004; Ellison et al. 2010). However, once the galaxy pair is found within a high density environment, the strength of the SFR enhancement diminishes or becomes undetectable (Alonso et al. 2004, 2006; Baldry et al. 2006; Ellison et al. 2010). Clearly, galaxies are sensitive to their environment beyond the scale of their nearest neighbour. The question remains, how far beyond the nearest neighbour does environment matter? Is it merely a local density effect, or does cluster membership, with scales far beyond the local, also impact a galaxy’s evolution? This work will attempt to address this question.

Several density trends are well documented in the literature for low redshift galaxy samples. The morphology-density and colour-

* jscudder@uvic.ca

density relations describe the declining fractions of blue, late-type galaxies with increasing density (Dressler 1980; Postman & Geller 1984; Balogh et al. 1997, 1998; Martínez et al. 2002; Tanaka et al. 2004; Baldry et al. 2006). The overall distribution of star formation rates also correlates with density, with the average galactic SFR declining as density increases (Hashimoto et al. 1998; Poggianti et al. 2008; Kauffmann et al. 2004; Cooper et al. 2008). Interpretations of the SFR-density relation are complicated by the increasing fraction of low- (or non-) star forming elliptical galaxies as density increases. The contribution of early type galaxies will bias the average SFR to lower values at higher densities (e.g., Balogh et al. 2004).

The dependence of SFR on density becomes much less clear for only the star forming subsample of galaxies, with many conflicting interpretations. Some studies find that among the star-forming fraction, there is no residual dependence on density (Couch et al. 2001; Balogh et al. 2004; Tanaka et al. 2004; Weinmann et al. 2006; Patiri et al. 2006; Park et al. 2007; Peng et al. 2010; McGee et al. 2011; Ideue et al. 2011). According to these works, the observed decrease in SFR with increasing density is entirely due to the changing fraction of star-forming galaxies with density, and once this dependence is eliminated, the distribution of SFRs is independent of density. Other studies counter these results, finding that the population change is not enough to account for the entire SFR-density relation, and that a density dependence remains (Balogh et al. 1998; Pimblet et al. 2002; Gómez et al. 2003; Welikala et al. 2008). Moreover, the scale over which the SFR is influenced by its surroundings is widely debated. Many authors find that it is primarily on the local scale (generally considered to be of order 1 Mpc or less) that the residual SFR-density dependence is found (Hashimoto et al. 1998; Carter et al. 2001; Lewis et al. 2002; Kauffmann et al. 2004; Blanton et al. 2006; Blanton & Berlind 2007). By contrast, some studies indicate that the environment on scales of order several Mpc is of greater importance than that of sub-Mpc scales (Goto et al. 2003; Park & Hwang 2009).

A further probe into the scales involved in environmental effects comes from the gas phase metallicity, which, like the SFR, can be modulated by the gas supply (Ellison et al. 2008a; Mannucci et al. 2010; Lara-López et al. 2010; Yates et al. 2011). In samples of interacting pairs, changes in the gas phase metallicity and SFR are linked, and have been shown to respond to some of the same physical processes (Scudder et al. 2012). Theory offers the picture of an interaction triggering large scale gas flow from the outer regions of a galaxy to the centre, and the enhanced densities of gas sparking star formation (Mihos & Hernquist 1996; Barnes & Hernquist 1996; Barnes 2004; Rupke et al. 2010; Montuori et al. 2010; Torrey et al. 2012). In agreement with this theoretical picture, close galaxy pairs show enhanced SFRs (Larson & Tinsley 1978; Donzelli & Pastoriza 1997; Barton et al. 2000; Lambas et al. 2003; Alonso et al. 2004, 2006; Woods & Geller 2007; Ellison et al. 2008b, 2010) and diluted metallicities (Kewley et al. 2006; Ellison et al. 2008b; Michel-Dansac et al. 2008). This indicates that gas phase metallicities ought to change, as the SFRs do, with density. In confirmation of this idea, studies of galaxies in clusters and other dense environments have shown metal enhancement relative to the field (Mouhcine et al. 2007; Cooper et al. 2008; Ellison et al. 2009).

In this paper, we employ a new tactic to investigate the effects of large scale environmental dependences. We select two samples of galaxies with similarly high small scale densities, but with different large scale environments. To this end, we use the catalogue of 3491 compact group (CG) galaxies in 828 CGs presented in Mendel et al. (2011, henceforth M11) as a refinement on the sam-

ple of McConnachie et al. (2009, henceforth M09). Although the original CG selection criteria were designed to identify groups that are not part of a larger overdensity (Hickson 1982; M09), M11 find that the SDSS CG sample can be divided into two distinct populations. One population appears to be truly isolated, whereas the other population appears embedded within a large scale structure, but isolated from other galaxies within the group. M11 show that despite the strong differences in their large scale environments, the galaxies in these ‘embedded’ and ‘isolated’ groups have similar morphological properties. In this paper, we investigate the spectroscopic properties of the embedded and isolated CG galaxies, focussing on their star formation rates and metallicities. The photometric catalogue of CG galaxies is therefore cross-matched with a spectroscopic sample of emission line galaxies from the SDSS DR7 (Abazajian et al. 2009). In Section 2, we describe the sample selection, including metallicity and AGN calibrations. In Section 3, we describe our methods for quantifying differences between the isolated and embedded CG galaxies and a sample of control galaxies. In Section 4, we discuss the implications of our results, along with a comparison to previous works, and present our conclusions in Section 5.

We assume $\Omega_M = 0.3$, $\Omega_\Lambda = 0.7$ and $H_0 = 70 \text{ km s}^{-1} \text{ Mpc}^{-1}$.

2 SAMPLE SELECTION

Our spectroscopic sample is taken from the publicly available MPA-JHU SDSS DR7 catalogue¹ of 927,552 galaxies. This catalogue provides measurements of up to 12 emission lines per galaxy, corrected for stellar absorption lines and Galactic reddening. Of these lines, we will eventually require robust flux measurements to be present in $H\alpha$, $H\beta$, $[\text{OII}]\lambda 3727$, $[\text{OIII}]\lambda 4959, 5007$, and $[\text{NII}]\lambda 6584$ for metallicity calibrations². As some of these galaxies are not unique objects within the catalogue, we use the MPA-JHU’s duplicate catalogue³ to remove duplicate galaxies from the sample. In this section, we describe the quality control measures taken in order to select a reliable sample of star-forming galaxies with measurable metallicities.

2.1 Quality Control

In order to ensure that the flux measurements will be robust for subsequent metallicity calculations, careful checks were made on the quality of the flux measurements. As an initial step, all galaxies with zero and negative flux values were excluded. Flux values of zero were determined to be either due to clipped lines or due to the line being redshifted out of the spectral range of the SDSS. Negative flux values, by contrast, seemed to be largely due to poorly subtracted Balmer absorption.

A redshift cut was imposed on the galaxies to ensure that the spectral lines needed for the metallicity calibrations will not have been shifted out of the spectral range or into a region of the spectrum dominated by sky line residuals. The bluest wavelength of the emission lines needed in our analysis, $[\text{OII}]\lambda 3727$, dictates the

¹ Available at: http://www.mpa-garching.mpg.de/SDSS/DR7/raw_data.html

² Recently, Groves et al. (2011) have found that the $H\beta$ equivalent widths from this catalogue are systematically underestimated by 0.35\AA . We do not expect this to affect our results, as all our comparisons are relative, and the underestimation found is constant across the entire sample.

³ Available at http://www.mpa-garching.mpg.de/SDSS/DR7/Data/all_matches_dr7.dat

lower redshift limit. This line has to be redshifted at least to the lower limit of the SDSS spectra at 3800 \AA ⁴. At the other end of the spectrum, significant sky line residuals appear at $\sim 8000 \text{ \AA}$. We use $H\alpha$ to set the upper redshift, by requiring that $H\alpha$ cannot be shifted past 8000 \AA . These wavelength constraints result in a redshift range of $0.02 \leq z \leq 0.25$. Additionally, we require that the catalogue flag `z_warning` be set to 0; a non-zero value for this parameter indicates a bad redshift.

An inspection of the distribution of flux values for emission lines showed that both the flux values and their errors were bimodal with a prominent secondary peak at flux values $> 10^{-11} \text{ erg s}^{-1} \text{ cm}^{-2}$. A number of the galaxies with the highest flux values were visually inspected and the emission line fluxes were re-measured manually. The manually measured emission line fluxes were found to be within the bounds of the lower flux peak, indicating that the high flux values were spurious. The continuum fluxes and errors were also found to be bimodal. The secondary peak in the continuum error ($> 10^{-9} \text{ erg s}^{-1} \text{ cm}^{-2}$) pushes the continuum fluxes, and thus the line flux, to extremely large values. Imposing a cut around the main distribution of continuum flux errors eliminated the majority of the secondary (high value) flux peak. The remainder of the high fluxes were found to be associated with high flux errors, and imposing a flux error threshold eliminated the last remnants of the secondary peak in the flux values.

It is standard practice to impose a Signal-to-Noise (S/N) cut on emission line fluxes to ensure high quality metallicity determinations (e.g. Kewley & Ellison 2008). We adopt a fairly standard S/N cut of 5 on all emission lines needed for our metallicity calibrations. We also impose a $S/N > 5$ cut on the Balmer ratio (the ratio of $H\alpha$ to $H\beta$ flux) to minimize the scatter away from the theoretical Case B recombination limit. Our placement of the S/N cut in the Balmer ratio is motivated by the data; less stringent S/N cuts yield a rapid increase in the scatter in the Balmer ratio. However, increasing the severity of this cut would not significantly decrease the scatter, and would serve only to limit our statistics. As we expect some random scatter below the theoretical lower limit of 2.85, we permit 3σ scatter below the theoretical limit on the Balmer ratio (see Figure 1). This ensures that all Balmer ratios are reasonable, and does not exclude a large number of galaxies. A summary of the final quality control cuts is presented in Table 1.

With robust flux values in hand, we next correct for internal galactic reddening to obtain intrinsic fluxes, using the Small Magellanic Cloud (SMC) extinction curve presented in Pei (1992). $E(B-V)$ values for the SMC and the Milky Way are very similar at these wavelengths, so our decision to use the SMC curve does not affect our results.

2.2 AGN Removal

Before metallicities can be calculated, any galaxies containing an Active Galactic Nucleus (AGN) must be identified and excluded. AGN are known to alter emission line strengths, which makes any metallicity calculated for a galaxy hosting an AGN unreliable. The canonical method of discriminating between star-forming and AGN galaxies is through the use of emission line ratios (Baldwin et al. 1981; Veilleux & Osterbrock 1987). In particular, the most broadly used diagnostic plot is the so-called BPT diagram, after the Baldwin et al. (1981) work in which it was proposed, which plots

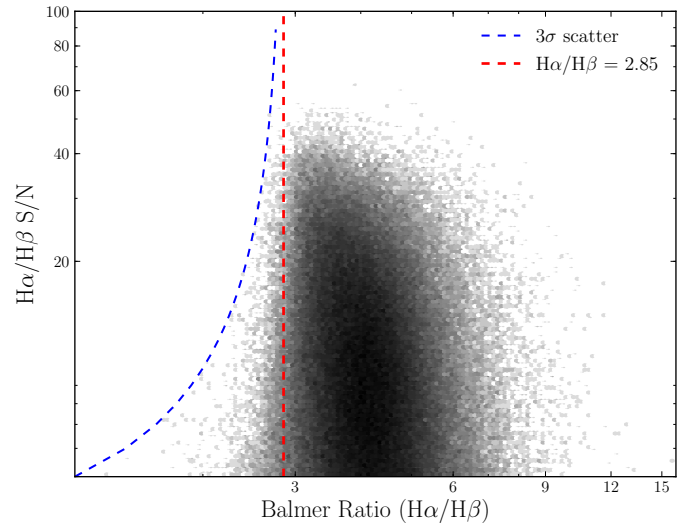


Figure 1. Final sample Balmer ratios vs. Signal to Noise for the quality controlled sample. Blue dashed line is the 3σ lower limit to the theoretical limit of 2.85 (red vertical line).

Final Quality Control	
Redshift	$0.02 < z < 0.25$
Continuum error	$10^{-19} < C_{err} < 10^{-15}$
Flux error	$10^{-19} < F_{err} < 10^{-13}$
$H\alpha/H\beta$ Signal/Noise	$S/N > 5$
Flux S/N	$S/N > 5$

Table 1. Final quality control parameters. Continuum and flux errors are in units $\text{erg s}^{-1} \text{ cm}^{-2}$. $H\alpha$, $H\beta$, $[\text{OIII}]\lambda 3727$, $[\text{OIII}]\lambda 4959, 5007$, and $[\text{NII}]\lambda 6584$ must pass these cuts to be considered a reliable detection in that line.

$[\text{OIII}]\lambda 5007/H\beta$ against $[\text{NII}]\lambda 6584/H\alpha$. The $[\text{OIII}]$ line is collisionally excited in both star-forming and AGN regions, so it cannot distinguish between the two ionisation sources, but rather serves as a metric for the strength of the ionisation field. $[\text{NII}]$, by contrast, originates in partially ionised regions, which are found preferentially around AGN sources due to the power-law radiation they produce. Photoionisation from O & B type stars does not produce a large partially ionised region, so the $[\text{NII}]$ line strength is relatively small in galaxies dominated by young stellar light. The combination of these two line ratios in the BPT diagram thus allows for differentiation between galaxies dominated by star formation and those with fluxes dominated by an AGN. In order for a galaxy in our sample to pass this diagnostic, it must have reliable detections in all four of the required emission lines.

There are a number of possible lines drawn on the BPT diagram to distinguish between star-forming and AGN. We select the diagnostic of Kauffmann et al. (2003b, K03). K03 is an empirical model, designed to follow the left-hand wing of the BPT diagram and is defined as follows:

$$\log([\text{OIII}]\lambda 5007/H\beta) = \frac{0.61}{\log([\text{NII}]\lambda 6584/H\alpha) - 0.05} + 1.30. \quad (1)$$

The K03 demarcation follows the star forming wing closely, so the fraction of AGN galaxies included in the SF sample should

⁴ We note that relaxing the redshift criteria from 0.02 to 0.01 does not increase the sample size of our final CG sample. (See Figure 3 of M11.)

be low; Stasińska et al. (2006) estimates only 3% contamination from AGN galaxies. We classify the sample of galaxies as star-forming or AGN based upon this diagnostic, resulting in a final star-forming sample of 126,756 galaxies.

2.3 Metallicity Calibrations

The metallicity calibration adopted here is the adaptation of the Kewley & Dopita (2002, henceforth KD02) recommended method presented in ?, KE08, which we refer to as the KD02-KE08 method. This calibration does not require the detection of as many strong lines (and in particular does not require the [SII] line), which helps to keep the final sample as large as possible. The KD02-KE08 calibration has low intrinsic scatter, and is easily converted into other metallicity calibrations without significant residuals.

The original KD02 calibration is based on photoionisation models and stellar population synthesis for high metallicities, and an average of R_{23} methods for low metallicities, where R_{23} is defined as

$$R_{23} = \frac{[\text{OII}]\lambda 3727 + [\text{OIII}]\lambda 4959 + [\text{OIII}]\lambda 5007}{\text{H}\beta}. \quad (2)$$

The modification implemented by Kewley & Ellison (2008) is in using a different set of R_{23} methods for the low metallicity galaxies. For high metallicities ($\log([\text{NII}]/[\text{OII}]) > -1.2$), the KD02-KE08 calibration is the same as presented in KD02. This calibration requires only [NII] and [OII] detections; as long as the galaxy is in the upper branch regime, we do not require any further strong line detections for the metallicity calibration. For $\log([\text{NII}]/[\text{OII}]) < -1.2$, the lower branch has changed from the original average of the Zaritsky et al. (1994) and McGaugh (1991) calibrations to an average of the Kobulnicky & Kewley (2004) and McGaugh (1991) lower branch calibrations, all of which are based on the R_{23} and O_{32} diagnostics, where O_{32} is defined as

$$O_{32} = \frac{[\text{OIII}]\lambda 4959 + [\text{OIII}]\lambda 5007}{[\text{OII}]\lambda 3727}. \quad (3)$$

The Kobulnicky & Kewley (2004) calibration takes an iterative approach, solving both for the ionisation parameter (defined as the number of ionising photons per number of hydrogen atoms) and the metallicity simultaneously. As these lower branch calibrations require the [OII] lines, galaxies that fall in the lower branch have the additional criteria that they must have significant detections in [OII] $\lambda\lambda 4959, 5007$.

2.3.1 Final Metallicity sample

Our final metallicity sample is 75,863 galaxies and represents both the sample with which we cross-match the CG sample and the basis of the pool from which we construct a control sample. The metallicity sample is significantly smaller than our initial star-forming sample because the metallicity calculation requires additional emission line detections beyond those required to classify the galaxy as star-forming. We take stellar mass⁵ values as calculated by the MPA/JHU group from fitting models to the 5-band SDSS DR7 photometry⁶. These masses are, in general, in good agreement with spectroscopically derived values calculated by Kauffmann et al.

⁵ Unless otherwise stated, all mass values in this work are stellar masses.

⁶ A discussion of their method is available at: http://www.mpa-garching.mpg.de/SDSS/DR7/mass_comp.html

(2003a). Star formation rates within the SDSS fibre (3'') are taken from Brinchmann et al. (2004), who use a set of 6 emission line fits to determine the SFR. Aperture corrected SFRs are also present in the catalogue. These SFRs are corrected from fibre to total values by calculating the galaxy light not contained within the fibre; by fitting models to the photometry of the galaxy outside the fibre, the aperture correction can be effectively made (See Brinchmann et al. 2004 for a full discussion of their aperture correction methodology). Salim et al. (2007) compare the results of this methodology with the SFRs obtained from UV flux, and find that for star-forming galaxies the two methods agree very well, with no bias introduced by the aperture corrections. We use the aperture-corrected SFR values for the rest of this work.

2.4 Compact Group Sample

Our parent CG sample consists of 3491 CG galaxies in 828 CGs (M11). This sample is a refinement of the Catalogue A of M09. Typical intergalactic distances within the groups are a few tens of kpc, ranging up to 140 kpc. The M09 CG sample applies a modification of the original criteria laid out by Hickson (1982) to the SDSS DR6, with isolation, minimum number of galaxies, and density requirements:

- (i) $N(\Delta m = 3) \geq 4$
- (ii) $\theta_N \geq 3\theta_G$
- (iii) $\mu_e \leq 26.0 \text{ mag arcsec}^{-2}$

$N(\Delta m = 3)$ is the number of galaxies within 3 magnitudes of the brightest galaxy within the group, μ_e is the surface brightness of the group, θ_G is the angular size of the group, and θ_N is the size of the circle beyond which there are no galaxies within the 3 magnitudes required for group membership. These criteria guarantee that there must be at least 4 galaxies in the group and the group itself must be separated by at least 3 times its own radius from any other equally bright galaxies. The surface brightness criterion guarantees the compactness of the group. Applying these criteria, M09 find 2297 CGs, containing 9713 galaxies, down to a limiting magnitude of $r = 18$. However, there is no redshift criterion in the identification process for these galaxies; galaxies identified as a CG are done so based only on their photometry, regardless of whether or not they have concordant redshifts. Approximately 50% of the original 9713 galaxies have reliable spectroscopic redshifts in the DR7 (M11).

In order to address the issue of false (due to projections) CGs in the M09 sample, M11 apply a statistical likelihood restriction to the master CG sample. Briefly, by looking at the probability density functions for the combinations of spectroscopic and photometric redshifts available for CG galaxies found within a given group, a large fraction of interloping galaxies can be removed. If this process of interloper rejection results in the group failing the richness criterion used to define the sample, the entire group is rejected. M11 estimate that there could be 20%-30% contamination remaining in the cleaned sample. M11 identified a distinction in the distribution of distances between the CG and the next nearest cluster or rich group. Approximately 50% of the cleaned CG sample can be classified as within $\leq 1 \text{ Mpc } h^{-1}$ of a rich group, using the Tago et al. (2010) catalogue compiled from the DR7 (see Figure 5 in M11). The other half of the sample is distributed at distances $> 1 \text{ Mpc}$ away from group structures. Placing a dividing line in the CGs at the minimum between the two distributions, M11 describe two populations: ‘embedded’ and ‘isolated’ CGs. We adopt this terminology for the galaxies residing within those groups. M11 shows that the galaxies residing within the two density bins have

systematically different photometric properties (i.e., an increase in the fraction of blue galaxies within isolated CGs).

We cross-match the galaxies belonging to either embedded or isolated CGs with our final metallicity and SFR sample to select only the galaxies residing in CGs that also have robust metallicities and SFRs. This cross-matching results in our final CG galaxy sample of 112 galaxies. Splitting the sample into embedded and isolated CGs results in 62 galaxies in isolated CGs, and 50 galaxies in CGs embedded within a large scale structure. For a list of the embedded and isolated CG galaxies and their properties, see Tables A1 & A2 respectively. SDSS thumbnails of 4 random embedded CGs and 4 isolated CGs are presented in Figures A1 & A2 respectively.

2.5 Matching to Controls

In order to make an effective comparison between our CG sample of galaxies and a control sample of galaxies, we must eliminate any major sources of bias. The three major sources of bias are stellar mass, redshift, and environment (Perez et al. 2009). As we are looking for an effect that varies with environment, we cannot match in that property, but we wish to match a control sample to the CG sample in stellar mass and redshift, such that the distribution of stellar mass and redshift in the control match the distributions in the CG sample. Our control pool is defined as any galaxy in the final metallicity sample that is not flagged as belonging to a CG.

Galaxies in our CG sample are matched to galaxies in the control pool simultaneously in total stellar mass and redshift, in a similar way to Ellison et al. (2008b). Briefly, this algorithm finds the best simultaneous match in mass and redshift to each galaxy in the CG sample. Once every galaxy has been matched to a control, a Kolmogorov-Smirnov (KS) test is used on the total distributions of the CG sample and control. If the KS test finds that the distributions are consistent with being drawn from the same parent distribution at $> 30\%$, then the matching continues without replacement until a maximum of 50 control galaxies have been matched to each CG galaxy in our sample, or the KS-test results in a probability $< 30\%$. Since the pool of possible control galaxies is large compared to the CG galaxy sample, the matching procedure reaches the full capacity of 50 matches per CG galaxy. Our final CG samples of 62 isolated CGs and 50 embedded CGs thus have control samples of 3100 and 2500 galaxies respectively. The masses and redshifts of the control galaxies are typically matched to within 0.05 dex and 0.003 respectively of the CG galaxy value. The E(B–V) values of the galaxies are found to be consistent between all four samples when a KS-test is applied.

The resulting normalised distributions of mass and redshift are shown in Figure 2. The control samples and the CG samples can be seen to match very well in both mass and redshift (the KS-test probabilities are $> 99\%$ between CG galaxies and their controls for both mass and redshift distributions). The embedded and isolated galaxies are also statistically similar to each other in both stellar mass and redshift, with KS-test values of 32.57% and 49.16% respectively.

3 OFFSETS IN THE SFR AND METALLICITY OF COMPACT GROUP GALAXIES

In this section, we present our methodology for finding and quantifying differences between the SFRs and metallicities of compact

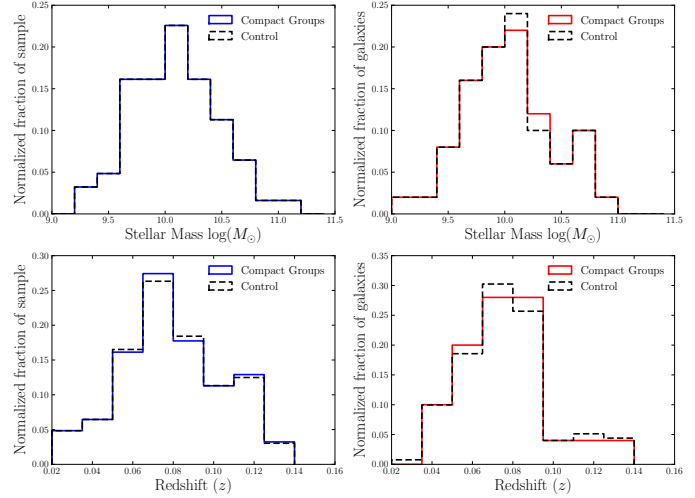


Figure 2. Normalized distributions of isolated (left panels) and embedded (right panels) CG galaxies and their controls for total stellar mass (upper panels) and redshift (lower panels). Galaxies are matched to controls in total stellar mass and redshift simultaneously until 50 control galaxies are matched to each group galaxy. KS-test probabilities that the samples are drawn from the same population are $> 99\%$ for the control and CG galaxy distributions in all panels.

group galaxies and their controls. We also present a set of bootstrap simulations to quantify the significance of a given measured offset.

3.1 Offset methodology

To quantify shifts away from the expected metallicities and SFRs at a given mass, we use a modification of the offset method from Patton et al. (2011). For each galaxy in the CG sample, we take the median (metallicity or SFR) value of all 50 control galaxies to which it was matched, and subtract that value from the observed value of the CG galaxy. An offset is therefore defined as:

$$\Delta \log(\text{O}/\text{H}) = (\log(\text{O}/\text{H}) + 12)_{\text{observed}} - \mu_{1/2} (\log(\text{O}/\text{H}) + 12)_{\text{controls}}, \quad (4)$$

$$\Delta \log(\text{SFR}) = \log(\text{SFR})_{\text{observed}} - \mu_{1/2} \log(\text{SFR})_{\text{controls}}, \quad (5)$$

where $\mu_{1/2}$ signifies the median. The calculated offsets are presented in Figures 3 and 4. The median metallicity offset for the isolated CG galaxies (solid vertical line in Figure 3) is -0.02 ± 0.04 dex (metal poor), whereas the embedded population has a median metallicity offset of 0.00 ± 0.02 dex (no offset; dashed vertical line). The uncertainty on the median is calculated using a jackknife technique. For each sample (embedded and isolated) the median offset is re-calculated by systematically removing one galaxy. For a sample of N galaxies, the jackknife error on the median is given by

$$\sigma = \sqrt{\frac{N-1}{N} \times \sum (\mu_{1/2}(N) - \mu_{1/2}(N-1))^2} \quad (6)$$

where $\mu_{1/2}(N)$ is the median value for the full sample of N galaxies, $\mu_{1/2}(N-1)$ is the median value for $N-1$ galaxies, and each of N galaxies is removed from the sample once.

The SFR offset distribution is shown in Figure 4; the embedded CG galaxies have SFRs that are lower than the control, with a median offset of -0.03 ± 0.05 dex. Isolated CG galaxies, by contrast, have a median offset of $+0.07 \pm 0.03$. Again, uncertainties are determined from the jackknife statistic.

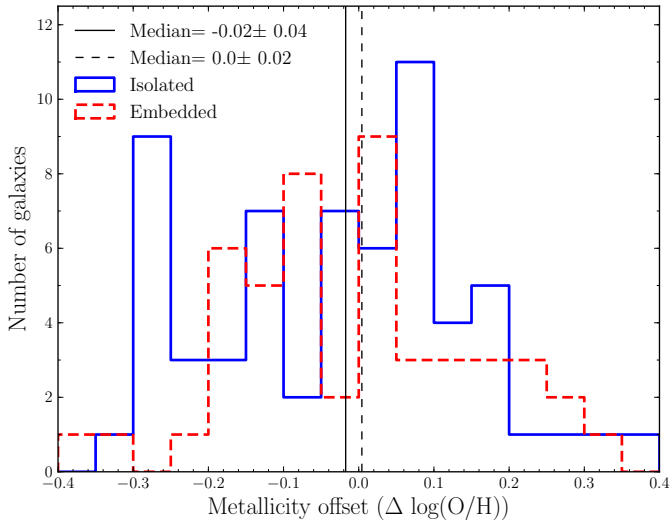


Figure 3. Offsets from the control MZR as defined by the median value per set of control galaxies for the embedded (red dashed line) and isolated (blue solid) compact group sample (50 and 62 galaxies, respectively). Black solid and dashed lines show the median offsets for the isolated and embedded compact group galaxies. Embedded galaxies show no median metallicity enrichment, contrasted with the median metallicity offset of isolated groups, which show a dilution of -0.02 ± 0.04 dex compared to the overall relation.

In order to determine whether the measured median offsets are strongly influenced by the errors on the SFRs, we use a Monte-Carlo resampling simulation to test the sensitivity of our results. We define a distribution of possible SFR values as a gaussian with mean of the original SFR, and with width defined as the 1σ errors on the SFRs, taken from Brinchmann et al. (2004). Median errors on any individual galaxy are ~ 0.1 dex. We draw new SFR values for both the CG and the control samples, and recalculate the offsets for the CG samples. We find that the median offsets are not significantly changed. After 10,000 iterations, the median $\Delta \log(\text{SFR})$ for isolated CG galaxies is 0.07 with a 1σ scatter in the distribution of 0.05. Embedded CG galaxies show a median $\Delta \log(\text{SFR})$ of -0.06 ± 0.06 (see Figure A3). These simulated median offsets and their uncertainties are consistent with the medians in Figure 4, and we conclude that the errors on the SFR measurements are not artificially enhancing the separation between the two samples.

The uncertainties on the median offsets indicate that the metallicities of the galaxies within both embedded and isolated CGs are consistent with a mass and redshift-matched control sample of non-CG galaxies. While the median SFR of the embedded CG galaxies is consistent with the control, the median SFR of the isolated CG galaxies is significantly offset from its control at $\sim 2\sigma$. Further, the isolated and embedded medians are significantly different from each other at the 1σ level.

3.2 Significance simulations for the SFRs

The jackknife technique estimates the statistical error on our samples of ~ 60 galaxies. However, we also want to quantify how often a given median offset will occur by chance (due to the intrinsic scatter in the SFR-mass relation). A random sample of 60 galaxies is therefore bootstrapped from the control sample 10,000 times. Recall that each control is one of 50 that has been matched to a given CG galaxy. When one of them is selected at random, the 49

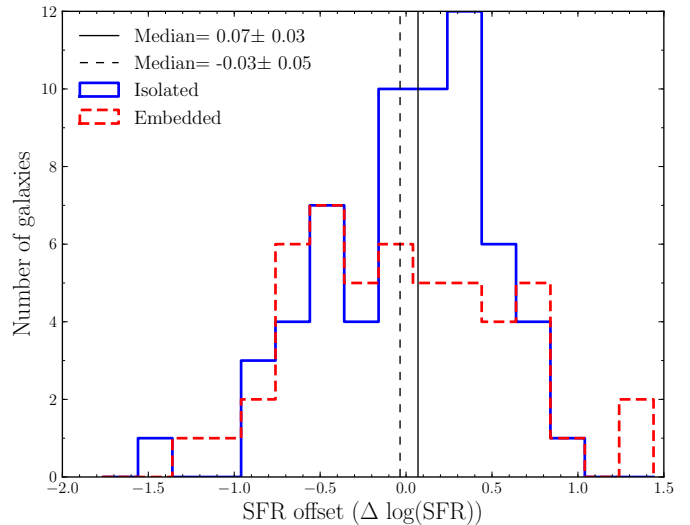


Figure 4. Same as Figure 3, but now showing the offset of CG galaxies from the SFR – mass relation. Isolated CGs show a median SFR enhancement of $+0.07 \pm 0.03$ dex, while embedded CG galaxies have SFRs depressed by -0.03 ± 0.05 dex below the control sample.

others in the set which are not selected as the ‘sample’ are left as the ‘control’. Offsets are then calculated between the randomly selected galaxy and each of the remaining controls. The median offset for the sample of 60 galaxies is determined, along with the jackknife error on that median. As the galaxies selected are part of the control pool, and no offset is artificially introduced, the majority of these offsets should be centred around zero. For each median, the significance σ is calculated by dividing the measured median offset by the jackknife error on the median. The fraction of the total number of runs with significant offsets (defined as $\sigma > 1, 2, 3,$ or 4) can then be calculated.

We can now compute for any given offset the fraction of the total number of bootstraps which returned significant medians at or beyond the offset being investigated. The results are shown in the top panel of Figure 5. The different lines indicate different values of σ . To compare to our results, the SFR enhancement seen in isolated CGs would be along the 2σ line. This simulation indicates that there is a 0.19% chance of detecting a SFR enhancement of $+0.07 \pm 0.03$ dex at random. We therefore conclude that the SFR enhancement we have detected, at its given observed significance, has a very low probability of occurring by chance due to scatter.

Whilst the above procedure assesses the probability that a given offset is found between the CG and control samples, we can also quantify the significance of the difference *between* the embedded and isolated samples. This is achieved by repeating the bootstrapping procedure described above, but this time selecting 2 separate samples of 60, and the absolute value of the difference in their median offsets is found. We then find the percentage of iterations where the simulated differences in median is greater than a given offset. The results of the two sample bootstraps are shown in the lower panel of Figure 5. The probability of a range of 0.10 dex between two samples drawn at random from the control SFR-mass relation is 0.67%, which corresponds to $> 2\sigma$ significance.

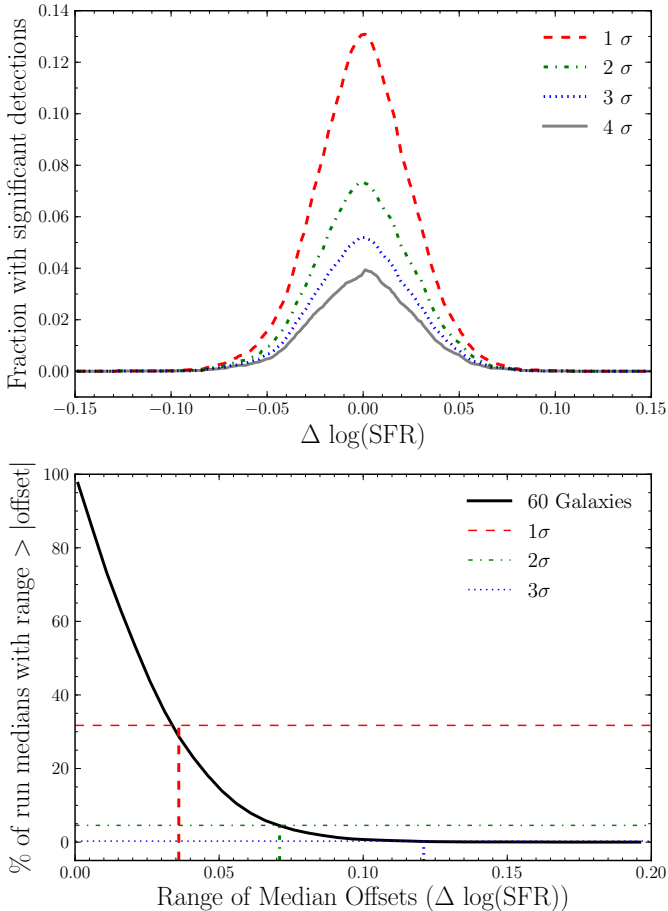


Figure 5. Results of the bootstrapping simulation for SFRs. A randomly selected sample of 60 galaxies is pulled from the control pool, and their offsets from their matched controls recorded, repeated 10,000 times. The top panel is the fraction of the total number of runs where a significant offset (i.e., $\sigma > 1, 2, 3,$ or 4) greater than a given offset i is found. Offsets of -0.04 and $+0.08$ dex at 2σ and 4σ significance have 2.14% and 0.02% likelihood of arising by chance, respectively. The bottom panel tests the percentage of times that a range in medians between samplings occurs; a difference in median of 0.10 dex could occur randomly $\sim 0.67\%$ of the time ($> 2\sigma$).

3.3 Upper limit simulations for metallicities

Although we find a statistically significant difference between the SFRs of embedded and isolated CGs, the metallicity offsets are inconclusive (-0.02 ± 0.04 and 0.00 ± 0.02 for isolated and embedded CGs respectively). Metallicity offsets in both embedded and isolated structures are statistically consistent with their control samples. To test the sensitivity of our null result given the sample size, we run a set of simulations similar to the bootstrap used in §3.2, but now introducing an artificial offset. In this simulation, 60 galaxies are randomly selected from the control sample and an artificial, single value offset (i) is added to all the metallicities of the selected galaxies. The resultant metallicities are then run through the offset calculation algorithm. Offsets are calculated between each of the 60 randomly selected galaxies and the remaining 49 in its matched set. The median measured offset (m) of the 60 galaxies is recorded. This step allows us to quantify the difference between the input offset i and the recovered offset m through our algorithm. We expect $i - m = 0$ if the sample can accurately recover the input metallicity offset. This bootstrap process is repeated 5,000 times. We calcu-

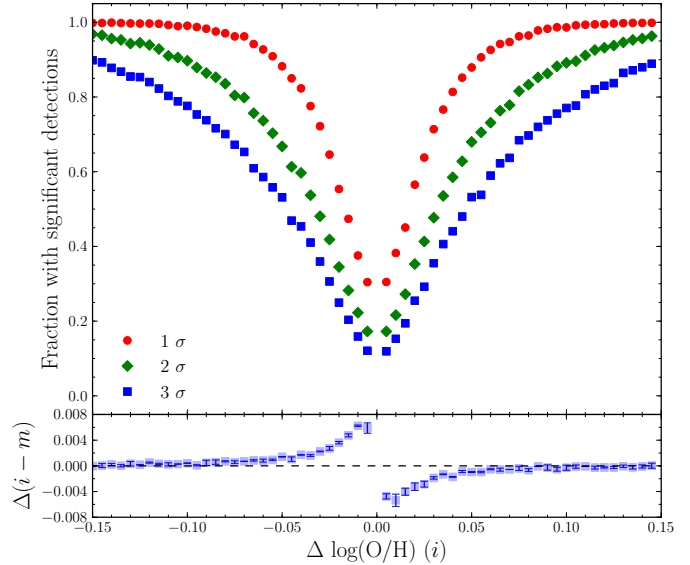


Figure 6. Results of the sensitivity simulation for the MZR offsets. Each point is the result of an independent simulation, bootstrapped 5,000 times. Each simulation selects a random sample of 60 galaxies from the control sample, and inserts an artificial offset i into the metallicities. The offsets are then calculated as normal, resulting in a measured offset m . The fraction of those runs which result in significant detections at the $1, 2,$ and 3σ level are plotted in black, red, and blue, respectively. The median difference between the measured offset m and the input offset i for the fraction of significant runs (at 3σ) is displayed as the blue squares in the lower panel as a function of i . Jackknife errors on the medians are smaller than the points.

late the jackknife error on each of the median values returned by the bootstrap. For each realisation, we calculate a significance σ by dividing the measured offset m by the jackknife error. We can then find the fraction of the total number of bootstrapped samples which return significant offsets for a given i . This fraction is then recorded, and plotted in the top panel of Figure 6. Red, green, and blue points reflect the fractions for $\sigma > 1, 2,$ and 3 , respectively. Each inserted offset requires a separate, independent run of 5,000 iterations of the bootstrap, and is plotted as a separate point in the figure.

In the bottom panel of Figure 6, the median difference between the input and measured offsets ($i - m$) is shown for those runs which returned significant medians at the 3σ level, as a function of the inserted offset i . This panel indicates that we are able to accurately recover an offset, if it is systematically different from the control. For values of i smaller than ± 0.05 , ($i - m$) shows an asymmetric shift away from zero. At very small i , it becomes increasingly unlikely for an offset m to be measured as significant. Therefore, those simulations which are measured as significant at small i are likely to be those which have scattered to median values further from zero. Negative values of i therefore preferentially return more negative values of m , and positive values of i return more positive values of m .

With these simulations as a base, we may compare the fractions of significant measured offsets returned by any given iteration of the bootstrap with the magnitude of offset we might expect to see. We use what has been found in previous studies of metallicity changes in high density environments as a guideline for reasonable magnitudes of offsets. The metallicity suppressions found in the pairs sample of Ellison et al. (2008b) and of Michel-Dansac et al.

(2008) are of order 0.05 dex, and the enhancements in overdensities in Cooper et al. (2008) are ~ 0.03 dex. Similar magnitudes are found by Ellison et al. (2009), who find offsets of 0.04 dex in galaxies in high density regions, relative to their control. Mouhcine et al. (2007) find slightly higher differences in metallicity of 0.06–0.08 dex between high and low density environments. For offsets in the range 0.03 – 0.05 dex, we find we only have a 34.8–51.1% chance of detecting a 3σ result. We do not reach 99% confidence levels of detecting a 1σ offset with our sample size until we reach offsets of 0.13 dex, which is much larger than anything previously discussed in the literature. The lack of significant metallicity offset in our CG sample may therefore be a limitation of our sample size. The fact that our metallicity results are both consistent with the control, combined with the results of this simulation, indicate our sample is unlikely to result in a significant offset of the magnitude suggested by the literature.

In summary, the offsets in SFR in our CG samples appear to be statistically distinct from each other, and galaxies in isolated CGs have significantly enhanced SFRs, whereas embedded CGs show no enhancement. However, the measured metallicity offsets are not sufficiently sensitive to probe metallicity differences between embedded and isolated compact group galaxies and their controls.

4 DISCUSSION

We have used the varying large scale environments of a consistently selected sample of compact, high density groups to probe the influence of the presence of a rich group or cluster. The compact group selection criteria allow us to select a consistently dense local environment on scales of ~ 100 kpc (see Figure 6 of M11) which, ignoring all external influences, ought to be subject to the same internal evolutionary processes. Galaxies in CG systems typically have small projected separations from each other; for our sample the median projected separation to the nearest neighbour is 46 kpc for both isolated and embedded samples. In galaxy pairs separations ≤ 30 kpc result in significantly enhanced SFRs (e.g., Barton et al. 2000; Lambas et al. 2003; Alonso et al. 2004, 2006; Ellison et al. 2008b, 2010; Scudder et al. 2012). Our sample has a significant population of galaxies with separations of this order, making galaxy–galaxy interactions an appealing explanation for the SFR enhancement seen in the isolated CG sample. The level of offset seen in our sample of isolated CG galaxies (+0.07 dex) may appear modest, but is comparable to studies of merger-induced star formation, which generally find median SFR enhancements of around +0.1 dex (e.g., Ellison et al. 2008b; Scudder et al. 2012). If the isolation criterion of the CG selection is effective at limiting outside influences, and interactions are the only dominant mechanism for transformations, we might expect both samples of CG galaxies to show consistent SFR enhancements over the control.

We find that galaxies in CGs in close proximity to a cluster or rich group (<1 Mpc) do not show the same preferential enhancement as their counterparts in isolated CGs. The embedded CG galaxies instead show consistency with the average galaxy in the control. Galaxies in isolated CGs (>1 Mpc from large scale structures), by contrast, show SFR enhancements over the control, consistent with the general trend presented by the SFR–density relation. This SFR disparity indicates that the local overdensities identified by the CG selection criteria cannot be considered in isolation. The presence of a nearby rich group exerts *some* influence on the star forming galaxies found within CGs, either by introducing an additional quenching mechanism, or because the galaxies within rich

groups are physically distinct from their isolated counterparts. The SFRs and metallicities of the galaxies within those groups therefore serve as diagnostics of the impact of the larger scale environment. *However, given the small magnitude of the difference between the two CG samples, the large scale environment does not appear to drive major changes in a galaxy’s evolution at fixed local density.*

4.1 Density scale dependences

Having determined the sensitivity and significance of the metallicity and SFR offsets, we wish to compare these results to previous work. However, previous metrics of environment usually fall into one of two categories; either an n^{th} nearest neighbour approach, or calculating galaxy density within annuli of increasing radius around a given point. In this work, we have used a new method of determining the large scale environment of a galaxy. Our division of galaxies into embedded and isolated systems is a binary assignment, based upon the presence (or lack) of rich group structure within a cylinder in redshift and projected separation space, centred upon the CG. This is an entirely different method of characterising the nature of a galaxy’s environment than has been typically used in the past.

Comparisons to the results found using existing measures of environment will require attention to the methodology of those metrics to be sure that they can probe the same kinds of overdensities. Since the n^{th} neighbour and annulus methods are calculated using entirely different algorithms, the meaning of the densities returned (as it applies to our CG sample) will vary, and comparisons to the results presented here must bear this in mind. In addition, most previous work has focused upon the *relative* importance of local and large scale dependences. This relative comparison is one that we cannot address in this work, as our classifications of embedded and isolated are not relative selections, and the local density - that of the CG itself - is relatively constant across our sample. Therefore, in comparing to previous work, we can only determine whether or not the previously obtained results are consistent with some level of SFR dependence on large scale environment as measured by our own method, to the extent that the density metrics may be compared.

The n^{th} nearest neighbour approach identifies high density regions of space by returning a shorter distance to the n^{th} neighbour in dense regions, and a longer distance in lower density regions (e.g., Hashimoto et al. 1998; Carter et al. 2001). Varying the value of n effectively changes the distance scales over which one wishes to probe the densities. With small values of n , the densities returned will be more reflective of local scale densities. Larger values of n will necessarily wander further afield to reach more distant neighbours. These distant neighbours will return a much larger volume of space over which to average the galaxy density, relative to their locally dense counterparts. The larger distances for isolated systems means that the densities derived from the identified n^{th} neighbour will be more reflective of a large scale density than those in locally dense environments (which return smaller distances), even if those local overdensities are relatively isolated from other structures (Weinmann et al. 2006). Since the distance to n^{th} nearest neighbour can vary smoothly from system to system, the distance scales being probed will also vary strongly as a function of local galaxy density. Furthermore, since the distance to n^{th} nearest neighbour is converted into a density, information about the distribution of those galaxies on scales less than that distance is lost. For the purposes of comparison to our metric, the n^{th} nearest neighbour algorithm simply needs to be able to distinguish between

isolated and embedded CG systems. Both isolated and embedded CGs have similar densities in the cores, but exhibit different galaxy surface densities on scales of 0.1 – 1 Mpc (M11). As long as the distances returned by the n^{th} nearest neighbour probe these scales, they should be able to distinguish between the isolated and embedded systems.

This relatively straightforward criterion for comparison with the n^{th} nearest neighbour provides a sharp contrast with the other main metric of galaxy density. The annulus approach is more difficult to compare to our method. In this approach, the galaxy density within annuli of increasing radius is measured (e.g., Lewis et al. 2002; Kauffmann et al. 2004; Blanton et al. 2006). Many works place their dividing line between ‘local’ and ‘large’ scale at 1 Mpc. The densities within the annulus of radius 1–3 or 1–6 Mpc is therefore used as their measure of large scale environment. 1 Mpc is also a natural dividing line in our sample, but only in the sense that this is the distance to the nearest group that distinguishes isolated and embedded CGs. The annulus approach is sensitive to the presence of broad overdensities beyond the distance of the defined ‘large scale’, generally 1–6 Mpc away from the selected galaxy. Our method provides the ability to define a system as embedded even when the overdensity is entirely on scales < 1 Mpc. In this case, the CG would still distinctly be embedded in a more massive halo than its own, but would not be distinguished as ‘large scale’ structure by an annulus of radius > 1 Mpc. If some fraction of the rich group extends beyond 1 Mpc distant from the CG galaxy, then it would be detected by the > 1 Mpc annulus. However, M11 shows that rich groups and CGs in any environment converge to similar galaxy densities at separations ~ 1 Mpc. With the median distance from CG centre to a rich group for embedded groups being of order ~ 0.3 Mpc, and the majority of rich groups’s strong galaxy surface density visible on scales < 1 Mpc, we might expect that only a small fraction of the galaxies within a rich group to extend beyond the 1 Mpc threshold. Furthermore, the annulus method loses all information on scales smaller than the area of the annulus. If an annulus contains an overdensity, but also contains a very low density region, these two extremes will average to a value that is not representative of either region.

With these differences in mind, we can now attempt to compare our results of a SFR dependence on large scale environment with previous studies. We emphasize that we are investigating only the dependence on those galaxies which are star forming relative to a star forming control, not the overall trend of star formation rate with density. Those works which conclude that the large scale environment affects the evolution of star forming galaxies by way of the cluster-centric radius (Park & Hwang 2009) or dark matter halo mass (Goto et al. 2003; Weinmann et al. 2006) are compatible with our results. However, a large body of work in the literature (using a mixture of methodologies) has concluded that the local scale effects dominate galaxy evolution (e.g., Hashimoto et al. 1998; Carter et al. 2001; Lewis et al. 2002; Kauffmann et al. 2004; Blanton et al. 2006; Blanton & Berlind 2007). These analyses consistently find a strong SFR dependence upon local galaxy density, with either very weak or absent dependence upon galaxy densities beyond the 1 Mpc scale. For example, Blanton et al. (2006) constrains the effects of large scale (1–6 Mpc) effects to be small, but does not exclude them as a minor contributor. Our results are not in disagreement with those studies which found that the local scales dominate galaxy evolution, consigning the large scale effects to a minor role. *The small difference in $\Delta \log(\text{SFR})$ between star forming galaxies in isolated and embedded CGs surely confirms the minor nature of the large scale environment. Our work indicates simply that there is*

a non-zero effect upon the galaxies within a larger structure beyond local density effects; it does not require that the effect must be the dominant one. Other works in the literature are less conservative, and interpret the lack of a strong dependence upon the galaxy densities at > 1 Mpc radii as evidence that the large scale environment does not have an effect upon a galaxy. Blanton & Berlind (2007) find that for the star forming fraction, large scale structure (defined as structure in an annulus > 1 Mpc) has no discernable effect upon the galaxy, with a bias in their measurement of no more than 5%, and density error of order 15%. Kauffmann et al. (2004) found that local densities dominate the SFR evolution; at low masses, the SFR of a galaxy was up to 10 times lower in high local densities than it was in low local densities. When testing the spatial scales between 1 – 3 Mpc, they found a very noisy relation in the 4000 Å break strength, their metric for SFR, with density: consistent with no dependence. In contrast, we have found that SFRs do depend, albeit at a low level, on their association with a large scale structure.

Reconciling our results with those in the literature likely comes down to the nature of the ‘environment’ identified by the different density metrics that have been previously used. Our division in environment identifies galaxies which are within 1 Mpc of a larger group than the CG itself. By the time scales of > 1 Mpc from the centre of a group are reached, the galaxy densities for isolated, embedded, and rich groups have all converged (M11). This indicates that most of the galaxy overdensity due to the rich group has also dwindled by 1 Mpc from the centre. If the groups are then sufficiently far away from the CG, they might cross over into the > 1 Mpc annulus, and be detected as an overdensity by that metric. However, the peak of the distribution of the distance to the nearest rich group is ~ 0.3 Mpc for embedded structures (M11). At 0.3 Mpc, the majority of the rich group will be found within 1 Mpc of the CG, and would not significantly increase the measured density for annuli > 1 Mpc. Therefore, even though the embedded CGs are situated in a significantly different environment than the isolated CGs, the overall galaxy density no longer reflects this difference at scales > 1 Mpc. Dividing environmental factors into large and local scale effects simply by using a cut in radius may blend extremely local drivers of evolution and some larger scale environmental factors. Our metric therefore cleanly separates those groups embedded in a more massive halo from those which are independent halos, no matter what the projected scale of the more massive group may be.

4.2 Physical Drivers

The interpretation of the difference between embedded and isolated galaxy SFRs depends on whether the galaxies are intrinsically and physically different when they are found within an overdensity, relative to in isolation, or whether the overdensity is imposing an additional processing mechanism on an initially similar set of galaxies. If the former, then galaxies found within large scale structure are reacting to the same set of evolutionary processes as galaxies in isolation, but their intrinsic properties make SFR enhancement (for example) more difficult to achieve.

One mechanism by which a physical difference in the galaxy populations between embedded and isolated CGs might arise is assembly bias (e.g., Croton et al. 2007; Cooper et al. 2010). Assembly bias states that galaxies in high mass potentials tend to be older, as they collapsed and began to cluster at earlier times. In this scenario, one might expect clusters to contain a higher fraction of old, so-called ‘red and dead’ galaxies, galaxies which have undergone many mergers, or galaxies which have been affected by the cluster potential through quenching mechanisms for a longer period

of time. Galaxies in rich groups tend to be preferentially gas poor (e.g., Chung et al. 2009) as a result. This framework offers one explanation for the SFR suppression in overdense regions. If galaxies within rich groups are simply older than their counterparts in the isolated groups, then they would be further along in their evolution, and may be further along the process of gas exhaustion and consumption. If the CG galaxies, due to their age, in addition to any environmental effects, are preferentially gas poor, then it will be significantly more difficult to trigger a SFR enhancement after an interaction (e.g., Alonso et al. 2006). Their isolated counterparts, having collapsed at later times, are younger, more gas-rich, and at a much earlier stage in their evolution; these galaxies will show SFR enhancements much more easily, as their gas reservoir is less depleted. This explanation does not require a difference in the mechanisms that modulate star formation rates in the two environments; the difference in intrinsic galaxy properties is enough to alter the galaxy's response to the same large scale environmental mechanisms. However, all the galaxies in our sample are emission line galaxies. While their star formation rates may be lower than the average galaxy, they still have significant amounts of gas. They cannot have been so affected by quenching and stripping mechanisms as to remove all their gas, if they can maintain strong emission lines. A large portion of the galaxies in our sample, regardless of their classification as embedded or isolated, retain relatively late-type morphologies (see Figures A1 & A2). The maintenance of the emission lines and their late-type morphologies limits the magnitude of the environmental and age-related evolution that the galaxies could have undergone.

Turning to consider processes that could alter the SFRs of a given galaxy in a different environment, we can eliminate quenching mechanisms that function on very small scales such as those associated with interactions; these should be consistently affecting both isolated and embedded systems. Whatever mechanism is preventing SFR enhancement in embedded CG galaxies must be associated with the larger scale cluster potential, and not simply with the high densities of the CG system. One explanation could be the difference in evolutionary processes in central and satellite galaxies. Galaxy populations divided in this way show that galaxies which are not the dominant galaxy in the dark matter halo undergo stronger environmental processes than the central galaxy does (Haines et al. 2006; Kimm et al. 2009; Peng et al. 2011; Tinker et al. 2011). Embedded CGs would, by definition, be a satellite halo within the larger cluster halo. The enhanced processing seen in most satellites would therefore be systematically applied to all galaxies in the embedded systems. Blanton & Berlind (2007) find that high density substructures (on scales of < 300 kpc) within a cluster are more correlated than expected with hosting red galaxies, i.e., these galaxies are further along in the quenching process. By contrast, the probability of the dominant galaxy in the potential being in our sample is significantly higher for isolated systems, where the CG environment is more likely to be an isolated halo.

If the difference between galaxies in isolated and embedded CG systems is not due to a systematic physical difference in galaxy population, then the galaxies in both systems ought to have begun their evolution in the CG as a roughly uniform population of galaxies. In order to explain the absence of the SFR enhancement seen in the isolated CG galaxies, an additional evolutionary force must be at work in embedded CG galaxies due to the cluster potential that is not in effect in isolated halos. This brings into suspicion the main drivers of galaxy evolution in clusters: ram-pressure stripping, galaxy-galaxy harassment, and strangulation. The isolation criterion for CG selection means that external galaxy harassment

is unlikely to be a significant influence. Galaxy harassment within the CG would contribute similar levels of evolutionary processing to both galaxy populations of CGs, and is therefore not a useful explanation for the difference in SFR response. Further, CGs have relatively low velocity differences, so harassment within the group itself is unlikely to dominate over lower velocity tidal interactions. This leaves ram-pressure stripping (removal of cold gas from the disk) and strangulation (removal of the external gas supply). Weinmann et al. (2006) argue that ram-pressure stripping should affect low mass galaxies more quickly, as they have a smaller potential and are more easily stripped of their gas, within a halo of given mass. This ought to result in a higher fraction of low mass early type galaxies relative to the fraction of high mass early types. Their sample, taken from the SDSS DR2, contradicts this prediction, finding no evidence for preferential changes to the lower mass galaxies. Wetzel et al. (2011) find that galaxies introduced into a larger halo can retain their SFR at pre-accretion levels for 1-2 Gyr before rapid quenching takes place; if ram-pressure stripping were the dominant mechanism, the galaxies would have their cold gas removed on much quicker timescales. Ram-pressure stripping is also excluded by a number of other authors (e.g., Tanaka et al. 2004; Blanton & Berlind 2007) due to the large radial extent of SFR suppressions, and SFR suppressions in low mass halos. Neither of these environments are expected to have the dense intra-cluster medium needed to support effective ram-pressure stripping (e.g., Rasmussen et al. 2008). This leaves strangulation as the prime suspect for SFR suppression in cluster environments, as it could still remove the hot halo of gas around a galaxy in lower density or lower mass environments (Balogh et al. 2000). Furthermore, it does not affect the morphologies or cold gas reservoirs of the galaxies involved (Weinmann et al. 2006). M11 find that the morphologies within embedded and isolated CGs are very similar, which also supports the idea of an environmental process being at work, rather than different evolutions due to age or gas exhaustion. Strangulation therefore appears to be an appealing mechanism for long-term suppression of SFR in emission line galaxies.

5 CONCLUSIONS

We present a sample of robustly calculated gas-phase metallicities and star formation rates for a sample of 75,863 star-forming galaxies in the SDSS DR7. These metallicities use emission line fluxes which passed rigorous quality control, and are cleaned of any AGN contribution. From this sample, we define a compact group sample of 112 galaxies that is uniformly selected on criteria for local richness and cleaned of likely interlopers. The compact group sample is further split by large scale environment into isolated and embedded subsamples, with 62 and 50 galaxies in each sample respectively. These two samples of star forming CG galaxies therefore have the same (very high) local density, but different large scale environments. The samples of compact group galaxies are simultaneously matched in mass and redshift with 50 non-compact group galaxies each in order to form robust control samples. By comparing the control samples with the compact group galaxy properties, we can measure the difference in the SFR and metallicity at fixed mass. The main conclusions of our work are as follows:

(i) Isolated and embedded compact group galaxies are offset from each other, and isolated CG galaxies are significantly enhanced relative to the field SFR-mass relation. Embedded galaxies do not show a similar enhancement. The SFRs of the galaxies in isolated CG systems show a median enhancement of $+0.07 \pm 0.03$

dex, whereas the galaxies in embedded systems show a median offset of -0.03 ± 0.05 dex. A series of bootstrap and Monte Carlo simulations indicate that this offset is robust. Our results indicate that, even though previous works have found a primary dependence on local density, the SFRs of star forming galaxies in locally overdense regions are mildly sensitive to large scale environment at fixed local density.

(ii) We find no evidence for a significant metallicity offset in either the isolated or embedded samples relative to their control samples. However, this non-detection is likely to be a result of small number statistics, as our sample is not likely to detect offsets of order 0.03–0.05 dex, which is the typical metallicity offset expected due to interactions or density driven effects. Our sample is therefore inconclusive with regards to the metallicity offsets. The simulations indicate that at 99% confidence we could have detected an offset of 0.13 dex.

Criteria classically used to select CGs define a consistent set of high density groups of galaxies. However, when these systems are divided according to the presence of a nearby cluster or rich group, the SFRs of the star forming galaxies within these systems become divided. The environmental split in median SFR demonstrates that large scale structure can exert an effect upon substructure found within it, even if at a low level, and that substructure is relatively isolated from other galaxies. The two possible explanations are: galaxies found within overdense regions are intrinsically different from galaxies in low density regions, which alters their response to the same local overdensities, or that the rich group structure imposes an additional evolutionary mechanism onto the galaxies in embedded CGs. This may give further support to the differences in satellite and central galaxy evolution, with strangulation, found only in cluster environments, as an effective process in slowly shutting down star formation.

ACKNOWLEDGMENTS

We thank the referee for useful comments which improved this paper. We also thank David Patton, Michael Balogh, Chris Pritchet, Alan McConnachie, and Bianca Poggianti for their comments on a draft of this paper.

We are grateful to the MPA/JHU group for access to their data products and catalogues (maintained by Jarle Brinchmann at <http://www.mpa-garching.mpg.de/SDSS/>).

Funding for the SDSS and SDSS-II has been provided by the Alfred P. Sloan Foundation, the Participating Institutions, the National Science Foundation, the U.S. Department of Energy, the National Aeronautics and Space Administration, the Japanese Monbukagakusho, the Max Planck Society, and the Higher Education Funding Council for England. The SDSS Web Site is <http://www.sdss.org/>.

The SDSS is managed by the Astrophysical Research Consortium for the Participating Institutions. The Participating Institutions are the American Museum of Natural History, Astrophysical Institute Potsdam, University of Basel, University of Cambridge, Case Western Reserve University, University of Chicago, Drexel University, Fermilab, the Institute for Advanced Study, the Japan Participation Group, Johns Hopkins University, the Joint Institute for Nuclear Astrophysics, the Kavli Institute for Particle Astrophysics and Cosmology, the Korean Scientist Group, the Chinese Academy of Sciences (LAMOST), Los Alamos National Laboratory, the Max-Planck-Institute for Astronomy (MPIA), the Max-Planck-Institute for Astrophysics (MPA), New Mexico State Uni-

versity, Ohio State University, University of Pittsburgh, University of Portsmouth, Princeton University, the United States Naval Observatory, and the University of Washington.

REFERENCES

- Abazajian, K. N., et al. 2009, *ApJS*, 182, 543
- Alonso, M. S., Lambas, D. G., Tissera, P., & Coldwell, G. 2006, *MNRAS*, 367, 1029
- Alonso, M. S., Tissera, P. B., Coldwell, G., & Lambas, D. G. 2004, *MNRAS*, 352, 1081
- Baldry, I. K., Balogh, M. L., Bower, R. G., Glazebrook, K., Nichol, R. C., Bamford, S. P., & Budavari, T. 2006, *MNRAS*, 373, 469
- Baldwin, J. A., Phillips, M. M., & Terlevich, R. 1981, *PASP*, 93, 5
- Balogh, M., et al. 2004, *MNRAS*, 348, 1355
- Balogh, M. L., Morris, S. L., Yee, H. K. C., Carlberg, R. G., & Ellingson, E. 1997, *ApJL*, 488, L75
- Balogh, M. L., Navarro, J. F., & Morris, S. L. 2000, *ApJ*, 540, 113
- Balogh, M. L., Schade, D., Morris, S. L., Yee, H. K. C., Carlberg, R. G., & Ellingson, E. 1998, *ApJL*, 504, L75
- Barnes, J. E. 2004, *MNRAS*, 350, 798
- Barnes, J. E., & Hernquist, L. 1996, *ApJ*, 471, 115
- Barton, E. J., Geller, M. J., & Kenyon, S. J. 2000, *ApJ*, 530, 660
- Blanton, M. R., & Berlind, A. A. 2007, *ApJ*, 664, 791
- Blanton, M. R., Eisenstein, D., Hogg, D. W., Schlegel, D. J., & Brinkmann, J. 2005, *ApJ*, 629, 143
- Blanton, M. R., Eisenstein, D., Hogg, D. W., & Zehavi, I. 2006, *ApJ*, 645, 977
- Brinchmann, J., Charlot, S., White, S. D. M., Tremonti, C., Kauffmann, G., Heckman, T., & Brinkmann, J. 2004, *MNRAS*, 351, 1151
- Carter, B. J., Fabricant, D. G., Geller, M. J., Kurtz, M. J., & McLean, B. 2001, *ApJ*, 559, 606
- Chung, A., van Gorkom, J. H., Kenney, J. D. P., Crowl, H., & Vollmer, B. 2009, *AJ*, 138, 1741
- Cooper, M. C., Gallazzi, A., Newman, J. A., & Yan, R. 2010, *MNRAS*, 402, 1942
- Cooper, M. C., Tremonti, C. A., Newman, J. A., & Zabludoff, A. I. 2008, *MNRAS*, 390, 245
- Couch, W. J., Balogh, M. L., Bower, R. G., Smail, I., Glazebrook, K., & Taylor, M. 2001, *ApJ*, 549, 820
- Croton, D. J., Gao, L., & White, S. D. M. 2007, *MNRAS*, 374, 1303
- Croton, D. J., et al. 2005, *MNRAS*, 356, 1155
- Donzelli, C. J., & Pastoriza, M. G. 1997, *ApJS*, 111, 181
- Dressler, A. 1980, *ApJ*, 236, 351
- Ellison, S. L., Patton, D. R., Simard, L., & McConnachie, A. W. 2008a, *ApJL*, 672, L107
- . 2008b, *AJ*, 135, 1877
- Ellison, S. L., Patton, D. R., Simard, L., McConnachie, A. W., Baldry, I. K., & Mendel, J. T. 2010, *MNRAS*, 407, 1514
- Ellison, S. L., Simard, L., Cowan, N. B., Baldry, I. K., Patton, D. R., & McConnachie, A. W. 2009, *MNRAS*, 396, 1257
- Gómez, P. L., et al. 2003, *ApJ*, 584, 210
- Goto, T., Yamauchi, C., Fujita, Y., Okamura, S., Sekiguchi, M., Smail, I., Bernardi, M., & Gomez, P. L. 2003, *MNRAS*, 346, 601
- Groves, B., Brinchmann, J., & Walcher, C. J. 2011, *ArXiv e-prints*
- Gunn, J. E., & Gott, III, J. R. 1972, *ApJ*, 176, 1

Haines, C. P., La Barbera, F., Mercurio, A., Merluzzi, P., & Busarello, G. 2006, *ApJL*, 647, L21

Hashimoto, Y., Oemler, Jr., A., Lin, H., & Tucker, D. L. 1998, *ApJ*, 499, 589

Hickson, P. 1982, *ApJ*, 255, 382

Hubble, E., & Humason, M. L. 1931, *ApJ*, 74, 43

Ideue, Y., et al. 2011, *ArXiv e-prints*

Kauffmann, G., White, S. D. M., Heckman, T. M., Ménard, B., Brinchmann, J., Charlot, S., Tremonti, C., & Brinkmann, J. 2004, *MNRAS*, 353, 713

Kauffmann, G., et al. 2003a, *MNRAS*, 341, 33

—. 2003b, *MNRAS*, 346, 1055

Kewley, L. J., & Dopita, M. A. 2002, *ApJS*, 142, 35

Kewley, L. J., Geller, M. J., & Barton, E. J. 2006, *AJ*, 131, 2004

Kimm, T., et al. 2009, *MNRAS*, 394, 1131

Kobulnicky, H. A., & Kewley, L. J. 2004, *ApJ*, 617, 240

Lambas, D. G., Tissera, P. B., Alonso, M. S., & Coldwell, G. 2003, *MNRAS*, 346, 1189

Lara-López, M. A., et al. 2010, *AAP*, 521, L53+

Larson, R. B., & Tinsley, B. M. 1978, *ApJ*, 219, 46

Larson, R. B., Tinsley, B. M., & Caldwell, C. N. 1980, *ApJ*, 237, 692

Lewis, I., et al. 2002, *MNRAS*, 334, 673

Mannucci, F., Cresci, G., Maiolino, R., Marconi, A., & Gnerucci, A. 2010, *MNRAS*, 414, 14

Martínez, H. J., Zandivarez, A., Domínguez, M., Merchán, M. E., & Lambas, D. G. 2002, *MNRAS*, 333, L31

McConnachie, A. W., Patton, D. R., Ellison, S. L., & Simard, L. 2009, *MNRAS*, 395, 255

McGaugh, S. S. 1991, *ApJ*, 380, 140

McGee, S. L., Balogh, M. L., Wilman, D. J., Bower, R. G., Mulchaey, J. S., Parker, L. C., & Oemler, A. 2011, *MNRAS*, 413, 996

Mendel, J. T., Ellison, S. L., Simard, L., Patton, D. R., & McConnachie, A. W. 2011, *MNRAS*, 418, 1409

Michel-Dansac, L., Lambas, D. G., Alonso, M. S., & Tissera, P. 2008, *MNRAS*, 386, L82

Mihos, J. C., & Hernquist, L. 1996, *ApJ*, 464, 641

Montuori, M., Di Matteo, P., Lehnert, M. D., Combes, F., & Semelin, B. 2010, *A&A*, 518, A56

Moore, B., Katz, N., Lake, G., Dressler, A., & Oemler, A. 1996, *Nature*, 379, 613

Mouhcine, M., Baldry, I. K., & Bamford, S. P. 2007, *MNRAS*, 382, 801

Park, C., Choi, Y.-Y., Vogeley, M. S., Gott, III, J. R., & Blanton, M. R. 2007, *ApJ*, 658, 898

Park, C., & Hwang, H. S. 2009, *ApJ*, 699, 1595

Patiri, S. G., Prada, F., Holtzman, J., Klypin, A., & Betancort-Rijo, J. 2006, *MNRAS*, 372, 1710

Patton, D. R., Ellison, S. L., Simard, L., McConnachie, A. W., & Mendel, J. T. 2011, *MNRAS*, 412, 591

Pei, Y. C. 1992, *ApJ*, 395, 130

Peng, Y., Lilly, S. J., Renzini, A., & Carollo, M. 2011, *ArXiv e-prints*

Peng, Y., et al. 2010, *ApJ*, 721, 193

Perez, J., Tissera, P., & Blaizot, J. 2009, *MNRAS*, 397, 748

Pimblett, K. A., Smail, I., Kodama, T., Couch, W. J., Edge, A. C., Zabludoff, A. I., & O'Hely, E. 2002, *MNRAS*, 331, 333

Poggianti, B. M., et al. 2008, *ApJ*, 684, 888

Postman, M., & Geller, M. J. 1984, *ApJ*, 281, 95

Rasmussen, J., Ponman, T. J., Verdes-Montenegro, L., Yun, M. S., & Borthakur, S. 2008, *MNRAS*, 388, 1245

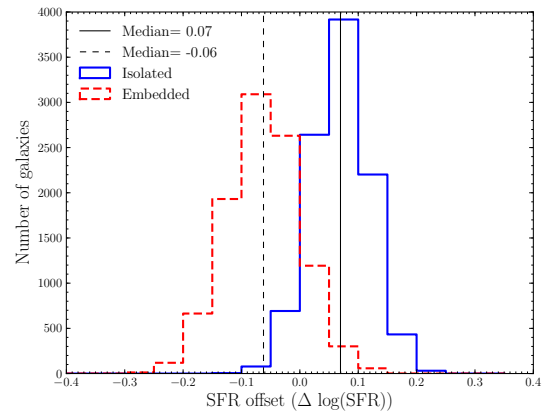


Figure A3. Results of a Monte-Carlo simulation on the SFR values of CG galaxies. The distribution of median offsets for the isolated (blue solid) and embedded (red dashed) CG galaxies is shown after 10,000 resamplings of the error distribution. Both control and CG galaxies were re-drawn, and their offsets recalculated. The median of the distribution of median offsets for isolated CGs is $+0.07 \pm 0.03$ dex, where the uncertainty is a 1σ width of the distribution. Embedded CG galaxies show median SFRs of -0.06 ± 0.06 dex. These distributions indicate that the effect of errors on the SFRs are not likely to change the results of our analysis. KS tests indicate a 0% chance that the two distributions were drawn from the same parent sample.

Rupke, D. S. N., Kewley, L. J., & Barnes, J. E. 2010, *ApJL*, 710, L156

Salim, S., et al. 2007, *ApJS*, 173, 267

Scudder, J. M., Ellison, S. L., Torrey, P., Mendel, J. T., & Patton, D. R. 2012, *MNRAS*, submitted

Skibba, R. A., et al. 2009, *MNRAS*, 399, 966

Stasińska, G., Cid Fernandes, R., Mateus, A., Sodré, L., & Asari, N. V. 2006, *MNRAS*, 371, 972

Tago, E., Saar, E., Tempel, E., Einasto, J., Einasto, M., Nurmi, P., & Heinämäki, P. 2010, *A&A*, 514, A102+

Tanaka, M., Goto, T., Okamura, S., Shimasaku, K., & Brinkmann, J. 2004, *AJ*, 128, 2677

Tinker, J., Wetzel, A., & Conroy, C. 2011, *ArXiv e-prints*

Torrey, P., Cox, T. J., Kewley, L., & Hernquist, L. 2012, *ApJ*, 746, 108

Veilleux, S., & Osterbrock, D. E. 1987, *ApJS*, 295

Weinmann, S. M., van den Bosch, F. C., Yang, X., & Mo, H. J. 2006, *MNRAS*, 366, 2

Welikala, N., Connolly, A. J., Hopkins, A. M., Scranton, R., & Conti, A. 2008, *ApJ*, 677, 970

Wetzel, A. R., Tinker, J. L., & Conroy, C. 2011, *ArXiv e-prints*

Whitmore, B. C., & Gilmore, D. M. 1991, *ApJ*, 367, 64

Woods, D. F., & Geller, M. J. 2007, *AJ*, 134, 527

Yates, R. M., Kauffmann, G., & Guo, Q. 2011

Zaritsky, D., Kennicutt, Robert C., J., & Huchra, J. P. 1994, *ApJ*, 420, 87

APPENDIX A: FIGURES & TABLES

In the Appendix, we include additional figures and tables for illustrative purposes. Figures A1 and A2 show Sloan images of sample CGs from the embedded and isolated samples respectively. Tables A1 and A2 contain information on the embedded and isolated CG galaxies respectively. Figure A3 shows the results of the Monte Carlo simulation conducted in §3.



Figure A1. 4 embedded CG galaxies, selected at random. The images are centred on the galaxy in the spectroscopic sample (identified by SDSS objID in the lower left corner), and are approximately 200 arcseconds to a side.

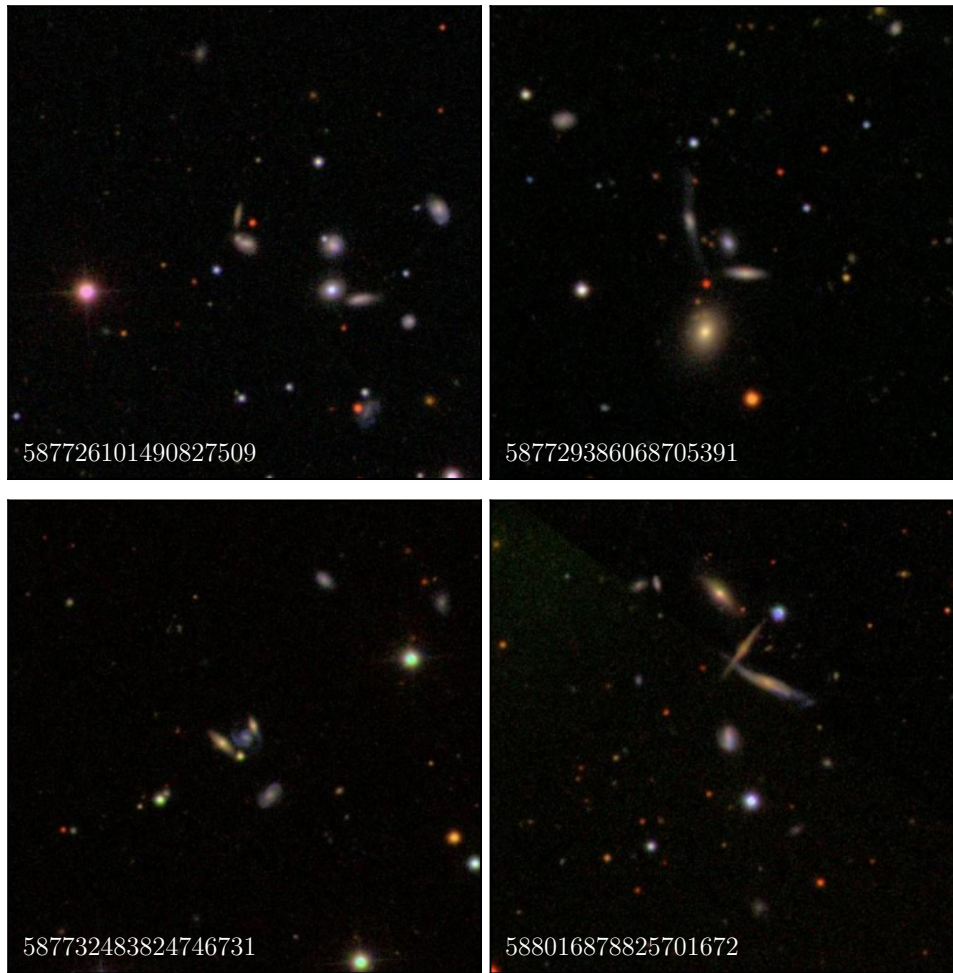


Figure A2. 4 isolated CG galaxies, selected at random. The images are centred on the galaxy contained in the spectroscopic sample (identified by SDSS objID in the lower left corner), and are approximately 200 arcseconds to a side.

SDSS ObjID	CG ObjID	Redshift	Stellar Mass	Metallicity	SFR
		z	$\log(M_*) (M_\odot)$	$12 + \log(O/H)$	$\log(\text{SFR}) (M_\odot \text{ yr}^{-1})$
587735348567736612	SDSSCGA00374.4	0.066	9.70	8.97	-0.23
587732470923591912	SDSSCGA02222.4	0.089	9.91	8.96	0.22
587742551749427305	SDSSCGA01310.2	0.072	10.09	9.09	0.58
587739629557907538	SDSSCGA00209.3	0.063	9.78	9.00	0.51
587736525909393590	SDSSCGA00436.4	0.109	10.79	9.29	1.59
587742614558212294	SDSSCGA00213.1	0.127	10.85	9.23	1.29
587731499184423092	SDSSCGA02083.4	0.050	9.52	8.96	-0.43
588017702397476999	SDSSCGA01110.2	0.067	10.02	9.04	0.34
587741600963297361	SDSSCGA00933.2	0.059	10.46	8.99	0.29
587729157905514683	SDSSCGA01012.4	0.069	9.64	9.01	-0.05
587736619327553911	SDSSCGA01186.2	0.089	10.13	9.03	0.61
587744727687954659	SDSSCGA01185.4	0.092	10.07	9.20	0.31
587729160048148639	SDSSCGA01232.2	0.091	9.88	8.94	0.38
587742551749427435	SDSSCGA01310.3	0.071	9.51	8.91	0.03
587742062159593500	SDSSCGA00253.2	0.077	10.15	9.17	0.72
587739648886505610	SDSSCGA00838.4	0.133	10.26	9.16	0.60
587741421632356738	SDSSCGA00979.4	0.051	9.59	8.99	-0.42
588017116128870540	SDSSCGA01825.1	0.071	10.04	8.96	0.62
588848901523439828	SDSSCGA01598.4	0.082	10.44	9.17	0.33
587729388223201436	SDSSCGA01434.3	0.035	9.80	9.11	-0.34
588017116128870551	SDSSCGA01825.2	0.071	10.22	9.24	0.42
587731891650494559	SDSSCGA02027.5	0.065	9.73	9.04	-0.06
587732578296529206	SDSSCGA00435.4	0.048	9.61	9.05	-0.46
587734894367539290	SDSSCGA01858.4	0.095	10.00	9.05	0.45
587741489294475468	SDSSCGA01272.3	0.042	9.17	8.71	-0.83
587738372745855292	SDSSCGA01487.3	0.096	9.98	9.00	0.47
587734894367539289	SDSSCGA01858.3	0.095	10.00	9.03	0.52
588017721713623164	SDSSCGA00494.1	0.082	10.69	9.31	0.96
587726033854398529	SDSSCGA01063.3	0.078	10.48	9.23	1.03
587745403074248994	SDSSCGA02266.3	0.116	10.32	9.05	0.48
588017979961901100	SDSSCGA00904.4	0.067	9.99	9.10	0.08
587739609162317939	SDSSCGA02209.3	0.078	9.72	8.97	0.17
587742060554879300	SDSSCGA01274.3	0.085	10.08	9.01	0.26
587736542020042979	SDSSCGA01833.2	0.059	10.10	9.12	0.02
587735696987586726	SDSSCGA01070.2	0.083	10.65	8.86	-0.44
587736584977711632	SDSSCGA02108.1	0.063	9.87	9.13	0.13
588017721713688616	SDSSCGA00494.3	0.082	9.93	9.01	0.23
587742060554944652	SDSSCGA01274.4	0.082	10.66	9.07	0.74
587735696987586734	SDSSCGA01070.4	0.082	10.38	9.31	0.58
587741600963297386	SDSSCGA00933.4	0.059	9.97	9.11	0.10
587731869627252855	SDSSCGA02011.4	0.140	10.31	9.15	0.85
587733429770846395	SDSSCGA01195.2	0.073	10.70	9.29	0.87
58773806565334220	SDSSCGA01301.2	0.077	10.20	9.14	0.65
587741490354389310	SDSSCGA01109.4	0.091	10.08	9.13	0.43
588023722317840542	SDSSCGA00728.4	0.044	9.30	8.91	-0.41
588023722317840548	SDSSCGA00728.3	0.044	9.90	9.07	-0.29
587745403074314378	SDSSCGA02266.4	0.116	10.04	9.10	0.22
587733429770911869	SDSSCGA01195.4	0.074	9.56	8.91	0.05
588016891713880190	SDSSCGA01137.3	0.056	9.64	9.11	-0.22
587735348025819263	SDSSCGA01108.4	0.054	9.81	9.15	0.06

Table A1. Embedded Compact Group galaxy properties. SDSS Objid is the unique identifier for that galaxy within Sloan, CG Objid is the Galaxy ID from the M09 catalogue where numbers before the decimal indicate the group ID, and the number after the decimal varies between galaxies within one group. Metallicities calculations are described in §2.3. SFR values come from the calculations of Brinchmann et al. (2004).

SDSS ObjID	CG ObjID	Redshift	Stellar Mass	Metallicity	SFR
		z	$\log(M_*) (M_\odot)$	$12+ \log(O/H)$	$\log(SFR) (M_\odot \text{ yr}^{-1})$
587739844854939883	SDSSCGA01177.2	0.114	10.61	9.10	0.82
588023720707424428	SDSSCGA01088.4	0.061	10.11	8.98	-0.51
587736975813836873	SDSSCGA00878.2	0.030	9.97	9.22	0.72
587739405707116711	SDSSCGA01128.1	0.054	10.48	9.04	0.41
587732471457186108	SDSSCGA00146.1	0.041	10.24	9.21	0.13
58772552264479032	SDSSCGA01533.2	0.066	10.16	9.18	0.35
587726101490827509	SDSSCGA00370.4	0.085	10.25	9.23	0.57
587725980687925438	SDSSCGA02231.4	0.097	10.27	9.18	0.50
588017724946972875	SDSSCGA00942.4	0.083	9.79	8.87	-0.07
587735344792928602	SDSSCGA00422.5	0.046	9.23	8.92	-0.48
587732702864080970	SDSSCGA02097.1	0.052	9.67	8.87	0.39
587736543623446530	SDSSCGA00970.4	0.087	9.89	8.97	0.57
587725041698799708	SDSSCGA01076.4	0.063	9.61	8.87	0.12
587725041698799706	SDSSCGA01076.3	0.064	9.62	8.87	0.18
587729386610557106	SDSSCGA01836.3	0.072	10.08	9.09	-0.41
587739377773576383	SDSSCGA00513.3	0.079	10.13	9.19	0.49
587728930803744828	SDSSCGA00362.1	0.112	10.05	9.06	0.74
587745244704473323	SDSSCGA01087.3	0.045	9.84	9.03	-0.19
587742062678900857	SDSSCGA01309.3	0.068	9.69	8.80	0.07
587745245240295524	SDSSCGA00601.3	0.113	10.36	9.20	0.48
587739827674022085	SDSSCGA00041.2	0.072	10.39	9.23	0.82
587729386068705391	SDSSCGA00078.3	0.056	9.37	8.84	0.01
587739844310007987	SDSSCGA01088.3	0.061	9.93	9.02	0.06
587731886268088671	SDSSCGA01783.2	0.078	10.75	9.25	1.16
587745539432776118	SDSSCGA02092.1	0.052	9.48	8.80	-0.11
587742774022045799	SDSSCGA01953.4	0.104	9.88	8.99	0.34
587742550686368002	SDSSCGA00687.2	0.087	10.18	9.19	0.34
588017627221721269	SDSSCGA01937.2	0.074	10.25	9.07	0.64
588848899373072598	SDSSCGA00713.3	0.118	10.50	9.01	0.50
588017990162710837	SDSSCGA00718.2	0.139	10.84	9.32	1.11
587732483824746731	SDSSCGA00305.2	0.084	9.76	8.88	0.25
587742013820305436	SDSSCGA01570.2	0.106	9.95	8.90	0.84
587742577521000590	SDSSCGA01809.3	0.093	10.33	9.19	0.48
588017627221721251	SDSSCGA01937.3	0.074	10.09	9.11	0.53
588007006048485395	SDSSCGA00936.1	0.074	10.19	9.07	0.80
587736975813836874	SDSSCGA00878.3	0.031	9.71	9.16	-0.50
587738947198910752	SDSSCGA01170.2	0.043	9.71	8.94	-0.19
587734893827129437	SDSSCGA00945.1	0.060	10.56	9.16	0.79
587741720678826052	SDSSCGA00562.2	0.067	9.50	8.90	0.39
587726101490827456	SDSSCGA00370.3	0.086	10.20	9.00	0.56
587725469057351815	SDSSCGA01097.1	0.132	11.09	8.89	0.87
587736782540964307	SDSSCGA01542.3	0.124	10.69	9.27	0.76
587739115237015957	SDSSCGA01970.3	0.099	9.74	8.88	0.21
587739610230554751	SDSSCGA00820.2	0.073	10.20	9.09	0.37
588017627221721162	SDSSCGA01937.4	0.074	10.40	9.03	1.03
588848900472111426	SDSSCGA01473.2	0.076	10.11	9.18	0.48
587739405707116699	SDSSCGA01128.2	0.054	10.46	9.08	0.67
588848899392340185	SDSSCGA00476.3	0.093	10.44	9.21	0.62
587729407546228763	SDSSCGA02056.3	0.029	9.82	9.02	-0.46
587739811028992231	SDSSCGA01347.2	0.068	9.57	8.93	0.23
587722984441119019	SDSSCGA01703.2	0.120	10.36	9.13	0.74
587722984441119010	SDSSCGA01703.3	0.121	10.68	9.27	0.72
587736546852864070	SDSSCGA00337.4	0.069	9.79	9.01	0.49
587737810644697402	SDSSCGA01583.3	0.103	9.81	8.95	0.46
587742578054201471	SDSSCGA01218.3	0.099	10.53	9.20	0.52
588016878825701672	SDSSCGA00227.3	0.082	10.12	9.05	0.71
587739610230554752	SDSSCGA00820.3	0.072	9.91	8.92	0.35
588009368008261825	SDSSCGA02225.5	0.092	10.13	9.04	0.44
587738411408294053	SDSSCGA00614.3	0.079	10.00	8.93	0.33
587742013297131696	SDSSCGA01348.3	0.102	9.96	8.96	0.54
587741603095707807	SDSSCGA00610.3	0.081	10.08	8.99	0.19
58774277455508821	SDSSCGA01132.3	0.123	10.22	9.14	0.59

Table A2. Same as Table A1, but for the isolated CG galaxies